

Journal of
Astronomical Telescopes,
Instruments, and Systems

AstronomicalTelescopes.SPIEDigitalLibrary.org

Scintillation properties of strontium iodide doped with europium for high-energy astrophysical detectors: nonproportionality as a function of temperature and at high gamma-ray energies

Rose Schmitt Perea
Ann M. Parsons
Mike Groza
David Caudel
Suzanne F. Nowicki
Arnold Burger
Keivan G. Stassun
Todd E. Peterson

Scintillation properties of strontium iodide doped with europium for high-energy astrophysical detectors: nonproportionality as a function of temperature and at high gamma-ray energies

Rose Schmitt Perea,^{a,b,*} Ann M. Parsons,^c Mike Groza,^b David Caudel,^{a,b} Suzanne F. Nowicki,^{c,d} Arnold Burger,^{a,b} Keivan G. Stassun,^{a,b} and Todd E. Peterson^{a,e,f}

^aVanderbilt University, Department of Physics and Astronomy, 2401 Vanderbilt Place, Nashville, Tennessee 37240, United States

^bFisk University, Department of Life and Physical Sciences, 243 W.E.B. DuBois Hall, 17th Avenue North, Nashville, Tennessee 37208, United States

^cNASA Goddard Space Flight Center, 8800 Greenbelt Road., Greenbelt, Maryland 20771, United States

^dUniversities Space Research Association, NASA Goddard Space Flight Center, Building 28, W174, 8800 Greenbelt Road, Greenbelt, Maryland 20771, United States

^eVanderbilt University, Institute of Imaging Science, 1161 21st Avenue South Medical Center North, AA-1105, Nashville, Tennessee 37232, United States

^fVanderbilt University, Department of Radiology and Radiological Sciences, Nashville, Tennessee 37232, United States

Abstract. Strontium iodide doped with europium [$\text{SrI}_2(\text{Eu}^{2+})$] is a new scintillator material being developed as an alternative to lanthanum bromide doped with cerium [$\text{LaBr}_3(\text{Ce}^{3+})$] for use in high-energy astrophysical detectors. As with all scintillators, the issue of nonproportionality is important because it affects the energy resolution of the detector. We investigate how the nonproportionality of $\text{SrI}_2(\text{Eu}^{2+})$ changes as a function of temperature from 16 to 60°C by heating the $\text{SrI}_2(\text{Eu}^{2+})$ scintillator separate from the photomultiplier tube. In a separate experiment, we also investigate the nonproportionality at high energies (up to 6 MeV) of $\text{SrI}_2(\text{Eu}^{2+})$ at a testing facility located at NASA Goddard Space Flight Center. We find that the nonproportionality increases nearly monotonically as the temperature of the $\text{SrI}_2(\text{Eu}^{2+})$ scintillator is increased, although there is evidence of nonmonotonic behavior near 40°C, perhaps due to electric charge carriers trapping in the material. We also find that within the energy range of 662 keV to 6.1 MeV, the change in the nonproportionality of $\text{SrI}_2(\text{Eu}^{2+})$ is ~ 1.5 to 2%. © The Authors. Published by SPIE under a Creative Commons Attribution 3.0 Unported License. Distribution or reproduction of this work in whole or in part requires full attribution of the original publication, including its DOI. [DOI: [10.1117/1.JATIS.1.1.016002](https://doi.org/10.1117/1.JATIS.1.1.016002)]

Keywords: scintillator detectors; nonproportionality; gamma-ray detectors; Onsager mechanism; charge carriers; excitons.

Paper 14011 received May 31, 2014; revised manuscript received Sep. 16, 2014; accepted for publication Oct. 7, 2014; published online Oct. 28, 2014.

1 Introduction

High-energy (~ 1 MeV and above) detectors serve several important roles in space-based astrophysics missions, yet there are many aspects that still need to be improved. Specifically, detectors that may be built of materials that are low-cost, lightweight, and have the best sensitivity and energy resolution at x-ray and gamma-ray energies are the most ideal. Study of the cosmos at high energies has applications across a broad range of research in astrophysics and space science—from the gamma radiation of distant quasars and black holes, to the x rays of solar storms, to the radioactive decay of minerals in the soil of planets and surfaces of asteroids in our solar system. Similarly, *in situ* astrobiological and geological investigations of the chemical makeup of planet and asteroid surfaces is optimally performed by probing with pulsed neutrons and measuring the scattered neutrons and gamma rays in this energy range.¹ In this manner, mineralogical assays can be performed to a depth of tens of centimeters below the surface without the need to physically drill, a process that is costly in power consumption.

For scintillators in use as gamma or x-ray detectors, the ionizing event frees an electron, creating a number of electron-hole pairs roughly proportional to the energy of the ionizing radiation. Ideally, each electron-hole pair forms an exciton and then migrates to an activator site, where they recombine and emit a photon in the visible spectrum. These photons are then collected and converted to an electrical signal that is, ideally, proportional to the energy of the ionizing event, since the number of photons should be proportional to the ionizing energy. However, in reality, along each step of this process mitigating factors lead to a loss of excitons, photons, or reduction in the output signal.² This resulting nonproportionality in turn limits the energy resolution.

Indeed, while scintillators used as room temperature radiation detectors have advantages over wide bandgap semiconductors, their limiting factor, at present, is energy resolution. In general, the need for high energy resolution gamma spectrometers is twofold: (1) to recognize structure in spectra (such as the shape of the positronium line) and identify closely located energy lines and (2) improve sensitivity, as the signal-to-background ratio improves with better resolution and the peak identifiability improves even when one energy line is involved.³ For example, in the determination of the subsurface elemental

*Address all correspondence to: Rose Schmitt Perea, E-mail: rose.s.perea@vanderbilt.edu

composition of planets and asteroids application using conventional fast neutron activation analysis techniques, the critical advantage comes from both improved energy line identification and improved sensitivity.⁴

Strontium iodide doped with europium [$\text{SrI}_2(\text{Eu}^{2+})$] is a scintillator material that, in particular, shows promise for high energy resolution, as an FWHM energy resolution at 662 keV has been reported as good as $\sim 2.5\%$,⁵ close to the 2% of the semiconductor cadmium zinc telluride (CZT).⁶ An important question, therefore, is whether it is possible to improve the energy resolution of $\text{SrI}_2(\text{Eu}^{2+})$ to the point that it is even more competitive with CZT. This would lead to a scintillator with a resolution comparable to or better than that of a semiconductor, while less expensive to manufacture and with the capacity to grow much larger single crystals and, therefore, build more efficient detectors compared to those fabricated from semiconductors.⁷

Improving the energy resolution of $\text{SrI}_2(\text{Eu}^{2+})$ requires characterizing and better understanding the nonproportionality of the material's light yield. Indeed, some calculations show that, should nonproportionality be minimized, $\text{SrI}_2(\text{Eu}^{2+})$ would achieve a fundamental Poisson limit of 1.5% energy resolution.⁸

Nonproportionality is a well-known characteristic of scintillators^{9–11} and arises because the incoming photon can deposit its full energy in a variety of ways (e.g., Compton scattering, Auger electrons, etc.) in a cascade process, which causes variations in the amount of light produced within the detector,¹⁰ and the light-yield responses to the individual divisions of energy are not proportional to that energy.¹⁰ It is thought that the underlying cause of nonproportionality is connected to the details of transportation of electric carriers (electrons, holes, and excitons) within the scintillator.^{9,10,12,13} The link between the transportation of charge carriers and the amount of light that a scintillator produces (the luminosity of the scintillator) was originally quantified by Birk's equation.² Attempts at modeling nonproportionality generally begin with this form, or an empirically modified form of Birk's equation.² One of these modified forms used by Payne et al. incorporates the Onsager mechanism into their model for light yield of a scintillator.¹³ The Onsager mechanism is a recombination rate that depends on the Onsager radius (separation) where an electron and hole will no longer recombine; this is because the Onsager radius is the distance where the Coulombic and thermal energies are equal.^{13–15} While in the Payne et al. study it is implied that perhaps the Onsager radius is connected with a term that pertains to the intrinsic properties of the crystal (and is verified upon comparison to experimental data), we infer that it is possible that there is also a connection between the Onsager radius and nonproportionality. This is further detailed in Sec. 3.

To make progress in the effort to improve the nonproportionality and, therefore, the energy resolution of scintillators as a new cost-effective solution for high-energy astrophysical detectors, it is necessary to characterize how factors such as operating temperature and incoming photon energy affect the nonproportionality. Therefore, two studies with $\text{SrI}_2(\text{Eu}^{2+})$ are presented in this paper. One is a study of nonproportionality as a function of temperature. The other is a study of nonproportionality as a function of energy at high energies.

The response of $\text{SrI}_2(\text{Eu}^{2+})$ as a function of temperature has been investigated previously by Lam et al. and Alekhin et al. [both studies are specific to SrI_2 , doped and un-doped, with Eu^{2+} Refs. 16 and 17], and Boatner et al., who investigated

a variety of scintillators up to very high (400°C) temperatures.¹⁸ In the Lam et al. study, they focused on temperatures from 295 down to 5 K, while the Alekhin et al. study went from 80 to 600 K [for $\text{SrI}_2(\text{Eu}^{2+})$] at low energies (up to 100 keV). Our study differs from the above studies in that it focuses on the nonproportionality of $\text{SrI}_2(\text{Eu}^{2+})$ from 16 to 60°C using gamma-ray sources of energy ranging from 81 to 1275 keV. The focus of the study presented here is the shift of the photopeak with increasing temperature and its implication on how nonproportionality changes as a function of temperature (the Boatner et al. study does not focus on nonproportionality, only on the shift of the photopeak) at a higher temperature range than Lam et al. study and at higher energy ranges than Alekhin et al. Information on the nonproportionality in this energy and temperature range may add information to the underlying physical cause(s) of nonproportionality (such as Onsager mechanism, trapping, etc.).

The high-energy study is unique in that this is the first study of $\text{SrI}_2(\text{Eu}^{2+})$ at such high energies (to our knowledge). The reason for this experiment was to evaluate the $\text{SrI}_2(\text{Eu}^{2+})$ detector as a possible gamma-ray alternative to the lanthanum bromide doped with cerium [$\text{LaBr}_3(\text{Ce}^{3+})$] currently used in the Probing in-situ with Neutrons and Gamma-rays Instrument.¹⁹ An interest in an alternative to $\text{LaBr}_3(\text{Ce}^{3+})$ comes from the need to have a scintillator without any self-activity. $\text{LaBr}_3(\text{Ce}^{3+})$ contains self-activity due to the ¹³⁸La (Ref. 20) creating intrinsic photopeaks in the gamma-ray spectrum that increases the background noise and can further interfere with composition analysis if the particular element has a characteristic gamma ray near any of the intrinsic ones coming from the crystal itself.

Both experiments bring new regimes to the previous studies mentioned above. Studies of the electron response, such as Refs. 5, 13, and 16 (to name a few), based on Compton scattering are useful and simpler for probing the effect of nonproportionality on scintillator energy resolution, since the ionization avoids the cascade process that occurs with gamma-ray interactions in inner shell electrons. Studies of the gamma photon response and its temperature variation, while more complicated due to the cascade mentioned above, are directly relevant to high-energy (6 MeV) gamma spectroscopy applications. The experimental setup and results for these studies are shown in Sec. 2, followed by the discussion in Sec. 3, and conclusions in Sec. 4.

2 Experiments

2.1 Nonproportionality as a Function of Temperature

2.1.1 Setup

The experimental setup consists of (in order from top to bottom in Fig. 1) an outer aluminum sleeve, Teflon, a copper heater, a 0.6 cm³ $\text{SrI}_2(\text{Eu}^{2+})$ crystal encapsulated in an aluminum can, a hollow quartz optical rod (101 mm in length) inside a brass cylindrical core surrounded by copper tubing, and a Hamamatsu photomultiplier tube (PMT) (Ultra-Bialkali model R6231-100). The crystal was grown and encapsulated at Fisk University with an FWHM resolution of 3.9% at 662 keV when tested directly coupled to the PMT (without the light guide). While use of the light guide causes loss of scintillation light, resulting in degradation of the resolution, its use here is to separate the PMT from the heat being applied to the crystal (allowing

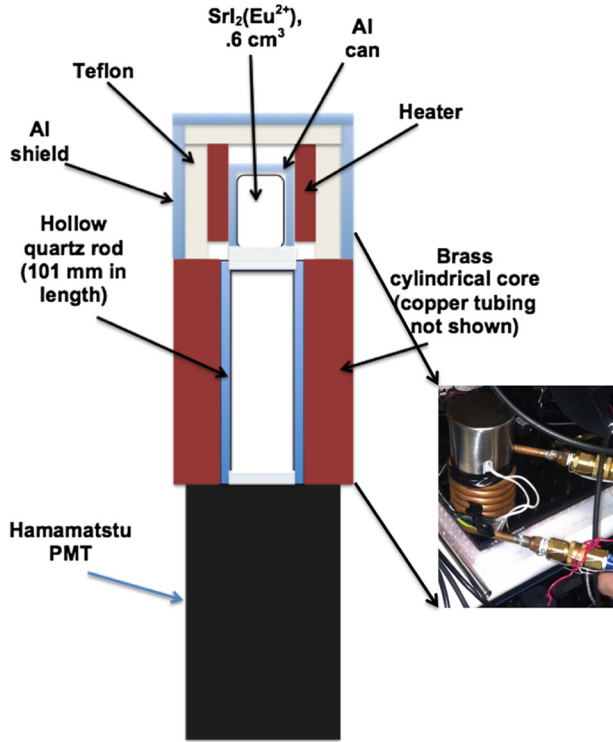


Fig. 1 Cross-sectional view of temperature experiment. Figure shows components of temperature study setup.

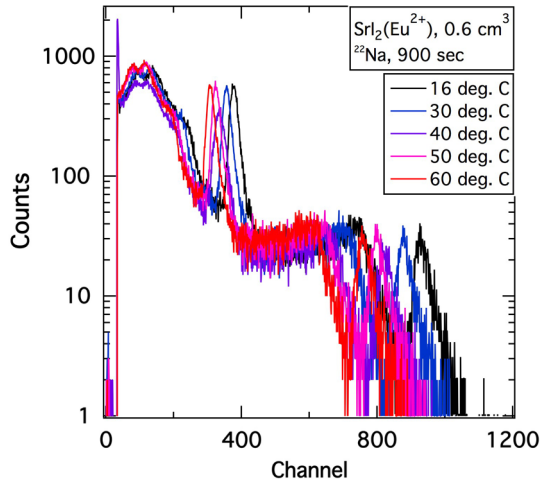


Fig. 2 $\text{SrI}_2(\text{Eu}^{2+})$ ^{22}Na spectra as a function of temperature. Figure shows the final run for each temperature with the ^{22}Na source. Notice that the photopeaks shift to lower channels with increasing temperature (please see color version online).

Table 1 Summary of averaged centroid values. Below are the weighted average centroid values [in analog to digital converter (ADC) channel] for each temperature.

| Energy (keV) | 16°C Mean (error) | 30°C Mean (error) | 40°C Mean (error) | 50°C Mean (error) | 60°C Mean (error) |
|--------------|-------------------|-------------------|-------------------|-------------------|-------------------|
| 81 | 61.524 (0.023) | 58.157 (0.061) | 55.803 (0.041) | 53.025 (0.035) | 50.540 (0.045) |
| 511 | 375.789 (0.613) | 356.011 (0.102) | 333.547 (0.781) | 323.848 (0.074) | 307.630 (0.057) |
| 662 | 487.596 (0.131) | 459.730 (0.082) | 439.375 (0.016) | 417.655 (0.058) | 396.787 (0.120) |
| 1275 | 925.454 (1.347) | 876.264 (0.389) | 821.248 (1.414) | 797.003 (0.696) | 757.137 (2.000) |

us to keep the PMT at room temperature). The inset in Fig. 1 shows the assembly of the top portion (everything except the PMT).

The method for acquiring data was done using the following three sources (energies ranging from 81 to 1275 keV): ^{133}Ba , ^{137}Cs , and ^{22}Na . The selected temperatures used were 16, 30, 40, 50, and 60°C. Counts from each source were collected for five consecutive runs at each temperature with the exception of ^{22}Na at 40 and 60°C. In the case of 40°C, there are only two runs recorded, and in the case of 60°C, there are only four. Each spectrum of the ^{133}Ba and ^{137}Cs sources was acquired for 300 s, while to achieve good statistics, the ^{22}Na spectra were recorded for 900 s.

2.1.2 Results

Figure 2 shows the full spectra of the final run at each temperature of the ^{22}Na source. As temperature increases, the 511 and 1275 keV photopeaks shift to lower channels. Only the ^{22}Na source is shown (for brevity), as the same behavior of the photopeak shifting to lower channels with increasing temperature is present for all the sources in all sets of spectra. All values are tabulated in Table 1. The centroid values shown in Table 1 are the weighted averages of all the runs for that energy and temperature.

The fitting and averaging routine that was used was written in Python, with the fitting routine making use of the Python function called `curve_fit()`.²¹ All the spectra are fitted with a Gaussian plus a polynomial (for the background continuum). To obtain the weighted average of the data, another function of Python, called `numpy.average()`²² was used.

Also, because of the light guide use, the resolution is reduced to $\sim 9.6\%$. This reduction in energy resolution and relative closeness of the 276 and 302 keV photopeaks of the ^{133}Ba source is unresolved, along with the 356 and 383 keV peaks. For this reason, we analyze only the 81 keV photopeak of the ^{133}Ba source along with the 511 and 1275 keV photopeaks of ^{22}Na , and the 662 keV photopeak of ^{137}Cs (which have no other source peaks nearby and are less affected) for the peak shifts and nonproportionality calculations.

To quantify the amount of shift in the photopeak, we performed a percent decrease calculation using 16°C as the reference temperature.

Relative shift (in %)

$$= \frac{\text{ADC Channel}_{\text{Temperature}} - \text{ADC Channel}_{16^\circ\text{C}}}{\text{ADC Channel}_{16^\circ\text{C}}} * 100\%, \quad (1)$$

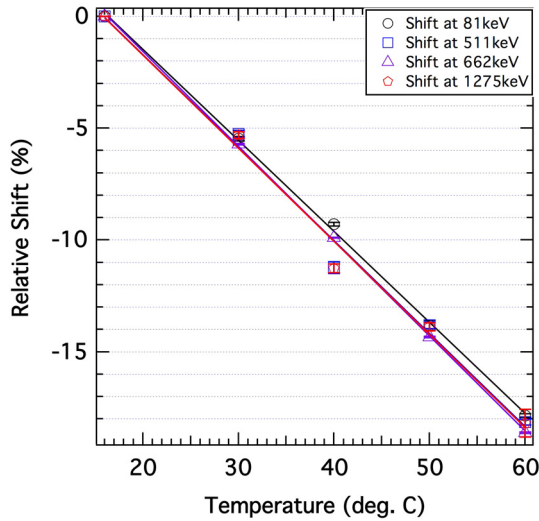


Fig. 3 Figure is a graphical representation of the relative shift of the centroid value at different energies, from a reference temperature of 16°C. Values can be found in Table 2. Each energy has a corresponding linear fit to the data points (please see color version online).

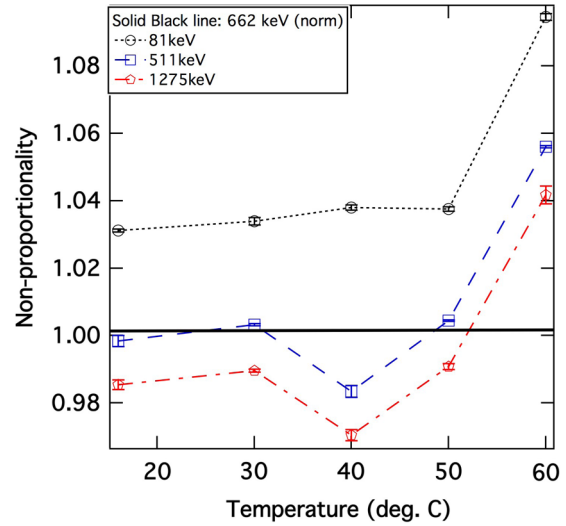


Fig. 4 Nonproportionality of $\text{SrI}_2(\text{Eu}^{2+})$ versus temperature. Figure shows the nonproportionality versus temperature, with data normalized to 662 keV at each temperature. The data points at 511 and 1275 keV are addressed in Sec. 3.1.

$$\sigma_{\text{Relativeshift (in \%)}} = \left[\left(\frac{1}{\text{ADCChannel}_{16^\circ\text{C}}} \right)^2 * \sigma_{\text{ADCChannel}_{\text{Temperature}}}^2 + \left(\frac{\text{ADCChannel}_{\text{Temperature}}}{\text{ADCChannel}_{16^\circ\text{C}}} \right)^2 * \sigma_{\text{ADCChannel}_{16^\circ\text{C}}}^2 \right]^{1/2} * 100\%. \quad (2)$$

The results are presented in Fig. 3 and Table 2. The percent decrease between energies, at each temperature (with the exception of the 511 and 1275 keV peaks of ^{22}Na at 40°C, which are addressed in Sec. 3), is 4 to 6%. This decreasing trend seen at all energies can be linearly fit. A possible explanation for this seemingly linear behavior is also addressed in Sec. 3.

Last, Fig. 4 shows the nonproportionality as a function of temperature. This is calculated by the following equations:

$$\text{Nonproportionality} = \frac{\text{ADC Ch\#}_{\text{Photopeak}} * \frac{662 \text{ keV}}{\text{ADC Ch\#}_{662 \text{ keV Photopeak}}}}{\text{Energy}_{\text{Photopeak}}}, \quad (3)$$

$$\sigma_{\text{Nonproportionality}} = \left\{ \frac{662 \text{ keV}}{\text{Energy}_{\text{Photopeak}}} * \left[\left(\frac{1}{\text{ADC Ch\#}_{662 \text{ keV Photopeak}}} \right)^2 * \sigma_{\text{ADC Ch\#}_{\text{Photopeak}}}^2 + \left(\frac{\text{ADC Ch\#}_{\text{Photopeak}}}{\text{ADC Ch\#}_{662 \text{ keV Photopeak}}} \right)^2 * \sigma_{662 \text{ keV Photopeak}}^2 \right]^{1/2} \right\}. \quad (4)$$

For all energy sources, the nonproportionality increases with the rise in temperature. This increase is ~6% overall. Tabulated values can be found in Table 3.

2.2 Nonproportionality at High Energies

2.2.1 Setup

As mentioned in Sec. 1, the second experiment was performed at the 6 MeV Gamma-ray Facility at NASA Goddard Space Flight Center with Dr. Ann Parsons and Dr. Suzanne Nowicki.²³ The setup for producing gamma rays is shown in Fig. 5. Piping surrounds the granite monument; starting from the left of the picture, the piping is wrapped in a helical fashion; this is where

Table 2 Relative shift of photopeak in $\text{SrI}_2(\text{Eu}^{2+})$. Tabulated values for the shift in photopeak of $\text{SrI}_2(\text{Eu}^{2+})$ as a function of temperature. Values correspond to Fig. 3.

| Energy (keV) | Between 30°C and 16°C Relative shift (in %) (error) | Between 40°C and 16°C Relative shift (in %) (error) | Between 50°C and 16°C Relative shift (in %) (error) | Between 60°C and 16°C Relative shift (in %) (error) |
|--------------|--|--|--|--|
| 81 | -5.468 (0.105) | -9.298 (0.075) | -13.813 (0.221) | -17.852 (0.079) |
| 511 | -5.262 (0.157) | -11.240 (0.253) | -13.821 (0.142) | -18.137 (0.134) |
| 662 | -5.714 (0.030) | -9.889 (0.024) | -14.341 (0.026) | -22.605 (0.033) |
| 1275 | -5.315 (0.144) | -11.259 (0.200) | -13.879 (0.187) | -18.624 (0.625) |

Table 3 Nonproportionality of $\text{SrI}_2(\text{Eu}^{2+})$. Tabulated values of the nonproportionality versus temperature as shown in Fig. 4.

| Energy (keV) | Nonproportionality (error) 16°C | Nonproportionality (error) 30°C | Nonproportionality (error) 40°C | Nonproportionality (error) 50°C | Nonproportionality (error) 60°C |
|--------------|----------------------------------|----------------------------------|----------------------------------|----------------------------------|----------------------------------|
| 81 | 1.031 (4.768×10^{-4}) | 1.034 (1.091×10^{-3}) | 1.038 (7.684×10^{-4}) | 1.038 (6.991×10^{-4}) | 1.041 (9.853×10^{-4}) |
| 511 | 0.998 (1.650×10^{-3}) | 1.003 (3.384×10^{-4}) | 0.983 (2.302×10^{-3}) | 1.005 (2.696×10^{-4}) | 1.004 (3.570×10^{-4}) |
| 662 | 1.000 (3.788×10^{-4}) | 1.000 (2.529×10^{-4}) | 1.000 (5.048×10^{-5}) | 1.000 (1.961×10^{-4}) | 1.000 (4.286×10^{-4}) |
| 1275 | 0.985 (1.458×10^{-3}) | 0.989 (4.743×10^{-4}) | 0.970 (1.672×10^{-3}) | 0.991 (8.762×10^{-4}) | 0.991 (2.634×10^{-3}) |

the pulsed neutron generator is placed. The piping goes across the top of the monument, to a water tank on the right side of the picture, and then comes back across (this is depicted in the schematic also included in Fig. 5). When the neutron generator is turned on, the neutrons excite the oxygen via the $^{16}\text{O}(n, p)^{16}\text{N}$ reaction. By the time the water has reached the tank, the ^{16}N decays releasing gamma rays of 2.7, 6.1, and 7.1 MeV (Ref. 24) (with probabilities of 0.82, 67, and 4.9%, respectively²⁵).

Also shown in Fig. 5 is the placement of the $\text{SrI}_2(\text{Eu}^{2+})$ detector. The $\text{SrI}_2(\text{Eu}^{2+})$ detector was loaned to us from Lawrence Livermore Laboratory and contains a 1 in. by 1 in. crystal [2.95% (19.5 keV) resolution at 662 keV] grown by Radiation Monitoring Devices. For a crystal of this size, we expect ~1 to 2% efficiency at 6 MeV. For the experiment, the $\text{SrI}_2(\text{Eu}^{2+})$ detector was grounded (with foil) and also wrapped in a foil sack to reduce interference from radio waves (used by other groups performing radar ranging at the NASA site). The placement of the $\text{SrI}_2(\text{Eu}^{2+})$ detector was ~20.5 (2) cm and acquisition time was 5 h.

2.2.2 Results

Figure 6 shows the resultant spectra of $\text{SrI}_2(\text{Eu}^{2+})$ of the 6 MeV experiment. A ^{137}Cs source was placed near the detector as a calibration source.

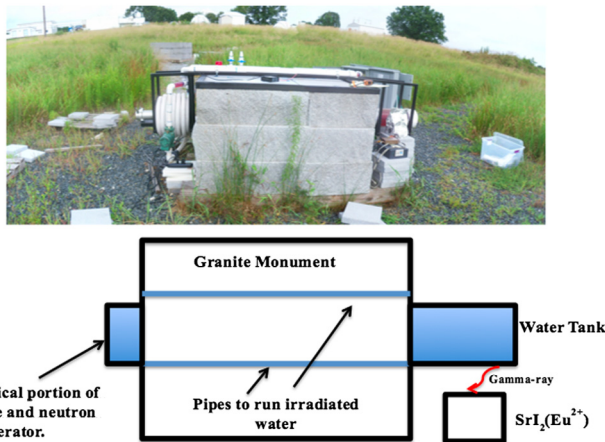


Fig. 5 6 MeV gamma-ray facility setup. Picture of the 6 MeV gamma-ray facility at NASA Goddard Space Flight Center. Neutron pulsed generator is on the left, and the water tank is on the right. Gamma rays are produced via the $^{16}\text{O}(n, p)^{16}\text{N}$ reaction. The schematic shows placement of neutron generator, water tank, and $\text{SrI}_2(\text{Eu}^{2+})$ detector for the experiment setup.

Last, the nonproportionality of $\text{SrI}_2(\text{Eu}^{2+})$ over the range of 662 keV to 6.1 MeV was calculated and is shown in Fig. 7 and in Table 4.

3 Discussion

3.1 Nonproportionality as a Function of Temperature

In Sec. 2.1, we presented the results of the nonproportionality of $\text{SrI}_2(\text{Eu}^{2+})$ as a function of temperature, see Fig. 4. In Fig. 4, the nonproportionality increases as the temperature increases, with the crystal most nonproportional at 60°C. This degradation is in agreement with the Alekhin et al. study (who found that the nonproportionality of their x-ray response became greater as they increased the temperature from 295 to 600 K).¹⁶ In comparison to the Lam et al. study, our higher-temperature measurements seem to still be in agreement with the lower-temperature data.¹⁷ Interestingly, those authors see a 5% degradation in nonproportionality as they decreased their temperatures from 295 down to 5 K with their lower-energy range¹⁷ of 31 to 41 keV. If we do the same comparison, we see an ~6% degradation in

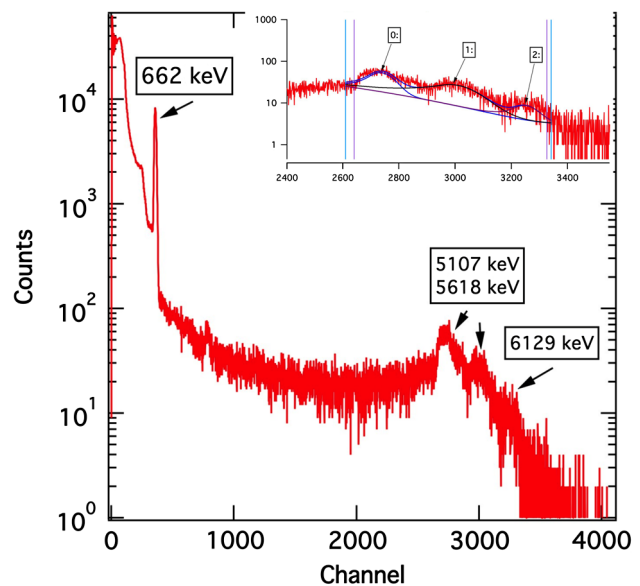


Fig. 6 Spectrum of ^{137}Cs , and 6 MeV gamma-ray sources obtained with $\text{SrI}_2(\text{Eu}^{2+})$. Peaks seen in the spectra are the ^{137}Cs photopeak, and the ^{16}O photopeak, see Ref. 24 (^{16}O escape peaks are also seen). Inset shows fits (Gaussian + polynomial) to these photopeaks (please see color version online).

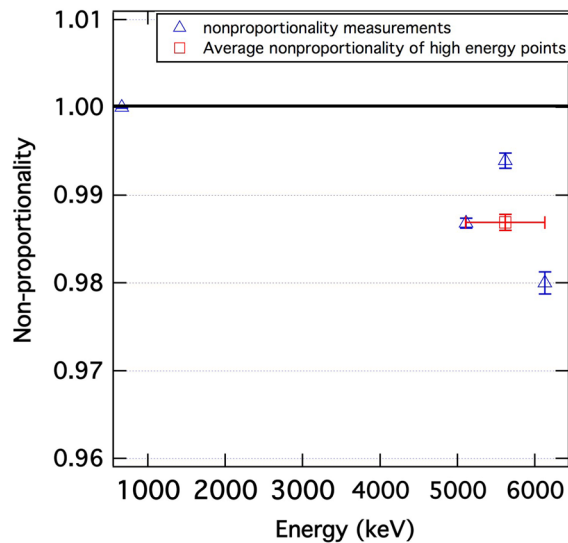


Fig. 7 Nonproportionality versus energy of $\text{SrI}_2(\text{Eu}^{2+})$, normalized to 662 keV. The red square (color version online) represents the average nonproportionality in the high-energy range. The error bars of this point in the x axis represent the range of energies measured, while the error bars in the y axis represent the true error in the nonproportionality. Values are shown in Table 4.

Table 4 Nonproportionality values of $\text{SrI}_2(\text{Eu}^{2+})$ at energies up to 6 MeV (normalized to 662 keV), along with the average nonproportionality (data point in red in Fig. 7). Energies of the $^{16}\text{O}(n,p)^{16}\text{N}$ reaction can be found at the National Nuclear Data website (see Ref. 24).

| Energy (keV) | Nonproportionality (error) | Energy resolution in % (error) |
|----------------|----------------------------------|--------------------------------|
| 662 | 1.000 (8.746×10^{-5}) | 4.842 (0.012) |
| 5107 | 0.987 (5.755×10^{-4}) | 3.955 (0.115) |
| 5618 | 0.994 ($8.751\text{E} - 04$) | 4.689 (0.179) |
| 6129 | 0.979 (1.272×10^{-3}) | 2.989 (0.278) |
| Average energy | Average nonproportionality | |
| 5618 | 0.987 (9.074×10^{-4}) | |

nonproportionality for our higher-energy range of 81 to 1275 keV as we increase the temperature from 16 to 60°C. From this comparison, it is clear that nonproportionality is indeed temperature dependent; however, whether the cause at lower temperatures versus higher temperatures is due to the same mechanism cannot be verified with this study.

To begin to understand the possible physical causes of these trends in Fig. 4, we observe in Figs. 2 and 3 and Tables 2 and 3 that there is a decrease in the amount of scintillation photons. Within the scintillator, there are many processes that can keep a scintillation photon from being produced (or delayed), such as radiation-less transitions to the ground activator states,² forbidden transitions in the activator states,² exciton–exciton annihilation,¹³ trapping,²⁶ and the Onsager mechanism¹³ (mentioned previously), to name a few.

The Onsager mechanism may provide a viable explanation for our results, as we see a decrease of scintillation photons

with increasing temperature. In the Payne et al.¹³ study, the Onsager mechanism, which states that the electron and hole need to be within a particular radius in order to recombine (from a balance of Columbic and thermal energies¹³), has an inverse relationship between that radius and temperature. This inverse relationship is seen in Fig. 3, where our data points have been fit to a linear equation for each energy. If in our study, the cause of less scintillation photons is due to the Onsager mechanism, then as we increase the temperature, the Onsager radius would decrease, making recombination more difficult with increasing temperature. Since the temperature was increased by the same fixed amount, the shift in channel number was decreased by the same amount.

Another possibility for the seemingly proportional behavior could be due to the mobilities of the electrons and holes. As the incoming photon ionizes the scintillator, the effects of electrostatic forces and thermal diffusion cause the charge carriers to separate. If the mobility of the charge carriers is low (or one of the charge carrier’s mobility is much greater than the other), the scintillator behaves nonproportionally.⁹ However, if both mobilities are high, then the scintillator behaves like a proportional crystal.⁹ Currently, there is no method to measure the mobility of charge carriers directly within a scintillator (as is done with semiconductors). If a method to accurately measure these mobilities is developed, then diffusion models, such as the one mentioned here, would help in interpreting these results. If the mobilities are indeed high (and perhaps more so at higher temperatures), then the condition imposed by the Onsager radius is never met for recombination.

Finally, the cause of the drop in our data points at 40°C with the 511 and 1275 keV peaks of ^{22}Na in Fig. 4 is not clear. There are indications of potential problems with the data run that produced the ^{22}Na measurements at 40°C (see Table 1 where only two measurements were obtained instead of five for most of the other runs).

3.2 Nonproportionality at High Energies

Over the energy range of 662 keV to 6.1 MeV, the $\text{SrI}_2(\text{Eu}^{2+})$ detector experiences only a small change in nonproportionality (1.5 to 2%). Previous measurements with $\text{LaBr}_3(\text{Ce}^{3+})$ have shown a similarly small change in nonproportionality of at most 2% over the energy range of 30 keV to 6 MeV.²⁷ Therefore, $\text{SrI}_2(\text{Eu}^{2+})$ appears to have a similarly good proportionality but without the detrimental effects of self-activity.

4 Conclusions

In this paper, we report findings from two different experiments on the nonproportionality of $\text{SrI}_2(\text{Eu}^{2+})$, motivated by the need to develop effective high-energy detectors with energy resolutions comparable to semiconductors for astrophysics applications and future space missions. One study was focused on the change in nonproportionality as a function of temperature; the other was focused on the nonproportionality at high energies.

In the temperature variation study, we found that the photopeak of the $\text{SrI}_2(\text{Eu}^{2+})$ crystal shifts to lower channels with increasing temperature and that the nonproportionality increases (up to 6%) with increasing temperature. This could be due to the charge carriers being at a distance equal to or larger than the Onsager radius as their kinetic energy is increased with the higher temperature. This increase in nonproportionality in temperature is in agreement with previous studies¹⁶ and also seems to be a trend when the temperature is decreased;¹⁷ whether

or not this is caused by the same mechanism is left for further investigation (and perhaps can be answered with further investigations of the mobilities of the charge carriers in the scintillator).

These results show that increasing temperature increases the nonproportionality; further investigation is needed to tie the specific cause (Onsager mechanism, trapping, and/or mobilities) and determine whether this cause is the same for high or low temperatures. Understanding this cause could give guidance into how to improve the growth (or perhaps correctly compensate for the effect in an already fabricated detector) so that this effect can be mitigated and energy resolution may be improved.

In the high-energy study, we found that $\text{SrI}_2(\text{Eu}^{2+})$ has a nonproportionality of $\sim 2\%$ at 6 MeV. Within the energy range of 662 keV to 6.1 MeV, the change in the nonproportionality of $\text{SrI}_2(\text{Eu}^{2+})$ is ~ 1.5 to 2% .

This is the first study of $\text{SrI}_2(\text{Eu}^{2+})$ at this energy regime, and these preliminary findings seem to be promising for applications in astronomy. If potential improvement in the nonproportionality of $\text{SrI}_2(\text{Eu}^{2+})$ is achieved, then $\text{SrI}_2(\text{Eu}^{2+})$ can become a viable detector with low background and no self-activity. This would enable lower-cost high-energy detectors deployable both in space-based platforms and in less temperature-controlled environments, such as planetary surface landers performing compositional analyses.

Acknowledgments

We would like to thank the two anonymous reviewers for their constructive criticism that helped improve this paper. One of the authors (R.S.P.) would like to acknowledge the financial support of the following: Graduate Opportunities at Fisk in Astronomy and Astrophysics Research (GO-FAAR) and the IGERT DGE-1069091 Neutron Scattering for the Science and Engineering of the 21st Century, support provided by the NSF grants, AST-0849736 (PAARE) as well as the support through NASA's 2012 Lunar and Planetary Science Academy at the Goddard Space Flight Center, and University of Maryland's 2013 Center for Research and Space Exploration in Space Science and Technology (CRESSST). We would like to thank Nereine Cherepy, Steve Payne, Patrick Beck, Scott Fisher, and Peter Thelin at LLNL for providing us with the packaged $\text{SrI}_2(\text{Eu}^{2+})$ detector and their guidance for the 6 MeV experiment. We would also like to thank Rastgo Hawrami and Kanai Shah at RMD Inc. for providing us the large $\text{SrI}_2(\text{Eu}^{2+})$ crystal that was used in fabricating the detector. One of the authors (R.S.P.) would also like to acknowledge the Fisk-Vanderbilt Masters-to-PhD Bridge Program and the Bridge Postdoc (Rudolfo Montez) for the support of this paper and in creation of the Python scripts utilized for the temperature data analysis.

References

1. J. G. Bodnarik et al., "Time-resolved neutron/gamma-ray data acquisition for in situ subsurface planetary geochemistry," *Nucl. Instrum. Methods Phys. Res. A* **707**, 135–142 (2013).
2. G. F. Knoll, *Radiation Detection and Measurement*, 3rd ed., John Wiley & Sons, Inc., Hoboken, New Jersey (1999).
3. G. Arantano, A. E. Bradley, and P. L. Phelps, "Sensitivity problems in biological and environmental counting," *IEEE Trans. Nucl. Sci.* **19**(1), 107–116 (1972).
4. M. Dallimore, G. Crossingham, and D. Ramsden, "High-resolution scintillation spectrometers for neutron-activation analysis," in *IEEE Nuclear Science Symp. Conf. Record*, Vol. 2, pp. 704–707, IEEE, Piscataway, NJ (2003).

5. N. J. Cherepy et al., "Scintillators with potential to supersede lanthanum bromide," *IEEE Trans. Nucl. Sci.* **56**(3), 873–880 (2009).
6. Y. Ramachers and D. Y. Stewart, "Energy resolution improvement in room-temperature CZT detectors," *J. Instrum.* **2**, P12003 (2007).
7. N. J. Cherepy et al., " SrI_2 scintillator for gamma ray spectroscopy," *Proc. SPIE* **7449**, 74490F (2009).
8. M. S. Alekhin et al., "Improvement of gamma-ray energy resolution of $\text{LaBr}_3:\text{Ce}^{3+}$ scintillation detectors by Sr^{2+} and Ca^{2+} co-doping," *Appl. Phys. Lett.* **102**(16), 161915 (2013).
9. W. W. Moses et al., "The origins of scintillator non-proportionality," *IEEE Trans. Nucl. Sci.* **59**(5), 2038–2044 (2012).
10. W. W. Moses et al., "Scintillator non-proportionality: present understanding and future challenges," *IEEE Trans. Nucl. Sci.* **55**(3), 1049–1053 (2008).
11. J. D. Valentine, B. D. Rooney, and J. Li, "The light yield nonproportionality component of scintillator energy resolution," *IEEE Trans. Nucl. Sci.* **45**(3), 512–517 (1998).
12. P. Dorenbos, J. T. M. deHaas, and C. W. E. vanEijk, "Non-proportionality in the scintillation response and the energy resolution obtainable with scintillation crystals," *IEEE Trans. Nucl. Sci.* **42**(6), 2190–2202 (1995).
13. S. A. Payne et al., "Nonproportionality of scintillator detectors: theory and experiment," *IEEE Trans. Nucl. Sci.* **56**(4), 2506–2512 (2009); S. A. Payne et al., "Nonproportionality of scintillator detectors. III. Temperature dependence studies," *IEEE Trans. Nucl. Sci.* **61**(5), 2771–2777 (2014).
14. G. J. Hoffman and A. C. Albrecht, "Near-threshold photoionization spectra in nonpolar liquids: a geminate pair based model," *J. Phys. Chem.* **95**(6), 2231–2241 (1991).
15. L. Onsager, "Initial recombination of ions," *Phys. Rev.* **54**(8), 554–557 (1938).
16. M. S. Alekhin et al., "Nonproportional response and energy resolution of pure SrI_2 and $\text{SrI}_2:5\%$ Eu scintillators," *IEEE Trans. Nucl. Sci.* **59**(3), 665–670 (2012).
17. S. Lam et al., "Nonproportionality and scintillation studies of $\text{Eu}:\text{SrI}_2$ from 295 to 5 k," *IEEE Trans. Nucl. Sci.* **59**(5), 2052–2056 (2012).
18. L. A. Boatner et al., "The characterization of scintillator performance at temperatures up to 400 degrees centigrade," *Nucl. Instrum. Methods Phys. Res. A* **709**, 95–107 (2013).
19. A. Parsons et al., "Active neutron and gamma-ray instrumentation for in situ planetary science applications," *Nucl. Instrum. Methods Phys. Res. A* **652**(1), 674–679 (2011).
20. W. J. Kernan, "Self-activity in lanthanum halides," *IEEE Trans. Nucl. Sci.* **53**(1), 395–400 (2006).
21. Scipy. Optimize. Curve_fit, Community, S., http://docs.scipy.org/doc/scipy-0.14.0/reference/generated/scipy.optimize.curve_fit.html (2013).
22. Numpy. Average, Community, S., <http://docs.scipy.org/doc/numpy/reference/generated/numpy.average.html> (2013).
23. J. G. Bodnarik et al., "Time-resolved gamma ray spectral analysis of planetary neutron and gamma ray instrumentation," in *Nuclear Science Symp. Conf. Record (NSS/MIC)*, pp. 1–6, IEEE, Piscataway, New Jersey (2010).
24. National Nuclear Data Center, Brookhaven National Laboratory, <http://www.nndc.bnl.gov/> (2013).
25. S. F. Nowicki, S. D. Hunter, and A. M. Parsons, "Development of a quasi-monoenergetic 6 mev gamma facility at NASA Goddard Space Flight Center," *Nucl. Instrum. Methods Phys. Res. A* **705**, 111–116 (2013).
26. M. Kapusta et al., "Non-proportionality and thermoluminescence of $\text{LSO}:\text{Ce}$," *IEEE Trans. Nucl. Sci.* **52**(4), 1098–1104 (2005).
27. P. Dorenbos, J. T. M. de Haas, and C. W. E. van Eijk, "Gamma ray spectroscopy with a circle divide 19×19 mm(3) $\text{LaBr}_3:0.5\%$ Ce^{3+} scintillator," *IEEE Trans. Nucl. Sci.* **51**(3), 1289–1296 (2004).

Rose Schmitt Perea is a graduate student at Vanderbilt University in the Physics and Astronomy Department. She received her BS in engineering physics (mechanical engineering option) in 2007 from New Mexico State University (NMSU), her MS in physics in 2010 from NMSU, and her MA in physics in 2013 from Fisk University. Through the Fisk-Vanderbilt Masters-to-the-PhD program, she has obtained experience with both scintillators/semiconductors and two internships at the NASA/Goddard Space Flight Center. This combination has prepared her in detector/instrument design for astrophysics.

Biographies of the other authors are not available.